Experimental and numerical investigation of the temperature and flow rate variation on an industrial high-temperature thermocline storage for recovering waste heat

Diane Le Roux, Aubin Touzo, Thibaut Esence, Régis Olivès

Experimental and numerical investigation of the temperature and flow rate variation on an industrial high-temperature thermocline storage for recovering waste heat

Diane Le Roux[1,2*], Aubin Touzo[1,3], Thibaut Esence[2], Régis Olivès[1,2]

[1] Laboratoire PROMES, CNRS, UPR 8521, Tecnosud, Rambla de la thermodynamique – 66100 Perpignan, France

[2] Université de Perpignan Via Domitia, 52 Avenue Paul Alduy, 66100 Perpignan, France

[3] SAS Eco-Tech Ceram, Espace Entreprises Méditerranée, Rue Edouard Belin, 66600 Rivesaltes, France

[*] Corresponding author: diane.leroux@promes.cnrs.fr

Abstract

For the valorization of industrial waste heat, the implementation of a thermal heat storage becomes essential. Since the waste heat fields show fluctuations in operating conditions, such as temperature and flow rate, a thermal energy storage must be able to accommodate these variations, by storing and then releasing this heat at constant temperature and flow rate. The aim of such a storage is to make the best use of the waste heat from industry. An industrial-scale high-temperature air/ceramic horizontal thermocline thermal energy storage (Eco-Stock®) has been tested through different operating parameters. The objective is to measure the influence of temperature and flow rate variations on the storage performance, in order to simulate a real heat ceramic process. The results revealed that the Eco-Stock® is able to store degraded heat fields and to restore heat at the average temperature of the heat field. As long as the characteristic time is an order of magnitude less than the charging time, the thermocline storage has a good energy performance. Despite gradual variations in temperature and flow rate during the charging process, the storage yield remains high and close to the reference storage (charging temperature of 525°C). Indeed, it reaches 66% for an outlet temperature of 350°C for all the temperature tests. For scenarios where the flow rate varies, the yield reaches up to 73.5% at 420°C. When heat is supplied from a ceramic manufacturing process, the Eco-Stock® can achieve a yield of 68%, which is 5.5% less than the reference case. In addition, the numerical model predicts the storage performances very accurately, proving its ability to absorb high temperature and flow rate constraints.

Keywords— Industrial waste heat, Thermocline, Packed-bed, Thermal energy storage, Industrial storage, Experimental, Numerical model

Highlights

- Influence of temperature and flow rate variations is investigated on an industrial-scale thermocline storage.
- The storage is able to smooth degraded temperature field by releasing it at the average field temperature.
- The industrial storage yield is weakly influenced by flow rate variations.
- The Eco-Stock® can transform a waste heat field into a controlled source of heat.
- Numerical model is very robust in absorbing large variations in its boundary conditions.

Nomenclature

Latin letters

A	Exchange area, m^2
c_p	Thermal capacity, $J \cdot kg^{-1} \cdot K^{-1}$
h	Convective heat transfer coefficient, $W \cdot m^{-2} \cdot K^{-1}$
h_v	Convective heat transfer coefficient per unit of bed volume, $W \cdot m^{-3} \cdot K^{-1}$
k	Thermal conductivity, J
Q	Energy, J
T	Temperature, K
t	Time, h
u	Interstitial fluid velocity, $m \cdot s^{-1}$
V	Volume, m^3

Greek letters

Δ	Variation
γ	Local storage yield
ϵ	Void fraction (Porosity)
ρ	Density, $kg \cdot m^{-3}$
τ	Load ratio

Subscripts

air	relating to air (heat transfer fluid)
bau	relating to the bauxite pieces inside the packed-bed (filler material)
c	relating to the low-temperature end of the storage
ch	relating to charging process
d	relating to discharging process
eff	effective value
end	relating to the end of a charging or discharging process
exc	exchanged between the inlet air and the system
ext	relating to external surface of the walls
max	maximal value
ref	relating to the reference condition
w	relating to walls of the storage tank

Acronyms

CSP Concentrated Solar Power
TES Thermal Energy Storage

1 Introduction

Most of the world's industrial energy demand is consumed as heat (70%) [1]. Nevertheless, the French Energy Agency (*Agence de l'environnement et de la maîtrise de l'énergie* (ADEME)) reports that up to 60% of this energy was wasted in the environment [2]. In Europe, 370 TWh/year are lost above 100°C [3]. In United States of America, waste heat represents up to 29% of the input energy in the glass, aluminium and foundry industries, from 200°C to 1700°C [4]. Industrial waste heat recovery is becoming essential to meet the Paris agreement [5] by improving industrial energy efficiency and reducing the environmental emissions.

Different technologies exist to valorize waste heat fields. It is important to identify the industrial process (iron and steel, cement, ceramics, food, glass-making, refineries) and its temperature level to choose the appropriate method to apply. Jouhara *et al.* [6] listed different technologies, their advantages, limitations and temperature range for various type of waste heat fields. Heat pumps can be employed to recover waste heat at low temperature [7]. This technology produces heat that can be used to produce domestic hot water for example. Low or medium-temperature waste heat can be recovered by means of thermodynamic cycles, such as Organic Rankine Cycle (ORC) [8, 9] and Kalina cycle [10]. Nemati *et al.* [10] proved that ORC is a better option than Kalina cycle for waste heat valorization. Some devices can also directly convert waste heat into electricity from low and medium temperature levels: Turbosol®, thermo-magnetic energy generation [11], and thermo-electric, piezoelectric, thermionic and thermo photo voltaic technologies [12]. To recover high-temperature waste heat, recuperators and boilers can be used [6, 13]. All these technologies have been integrated into industrial processes to improve their energy efficiency. Nevertheless, waste heat is intermittent, so the energy efficiency of these methods is reduced. To solve the mismatch between waste heat generation and energy consumption, Thermal Energy Storage (TES) is considered a key solution over a wide temperature range [14]. Manente *et al.* [15] proposed a structured procedure to automatically select the best TES in industrial waste heat recovery application. Several parameters are considered on the charging and discharging processes as well as on the storage. The application of their model showed that packed-bed storage seems to be better than sensible or latent storages, with more steam generated during the discharging step.

Packed-bed storage has grown considerably in recent years, particularly because of the use of a single tank and filler material can reduce the cost of the TES by up to 35% compared to a two-tank molten-salt storage [16, 17]. In the building sector, Fitó *et al.* [18] experimented with a low-temperature industrial waste heat recovery system consisting of a TES and a heat pump. In the industrial field, an air/steel slag packed-bed system had been used to recover waste heat from the inherent batch operation of electric arc furnace slag [19]. In the same field, Eco-Tech Ceram[1] developed a high-temperature thermocline TES to recover waste heat and inject it into another process in the plant [20]. In packed-bed storage, the thermocline zone has a significant impact on heat exchange. The performance and behavior of packed-bed TES is highly dependent on operating conditions. These conditions are imposed by heat fields during the charging step and by downstream process during the discharging step. Waste heat is not controlled and stabilized. The potential of the really exploitable waste heat depends on the temperature and flow rate levels, the power and the fluctuations in amplitude and frequency. It is important to know how to characterize this potential. In many cases, exhaust temperature and mass flow rate can vary over

[1] https ://www.ecotechceram.com

time, as illustrated in Figure 1. Therefore, a TES must be able to absorb variations in operating conditions during the charging process without excessively degrading its performance.

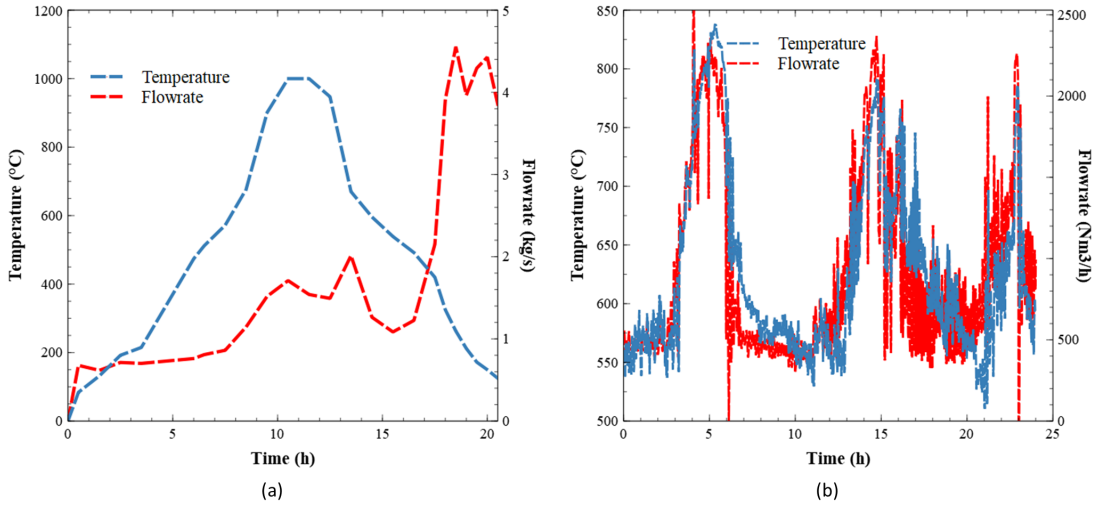

Figure 1: Example of waste heat field of a ceramic process (a) and a steel plant (b)

Some studies looked at the influence of several operating conditions on thermocline TES, with fluid velocity being the most studied to our knowledge in the literature [21–28]. Inlet velocity seems to play a minor role but affects storage performance. A low inlet velocity reduces the influence of the internal conduction resistance of the material by reducing the Biot number. But a too low velocity tends to increase the relative influence of thermal diffusion and heat loss, participating to the destratification of the thermocline [21, 22]. Bruch *et al.* [23] reported that increasing fluid velocity improves utilization ratio and storage efficiency with an experimental prototype and a numerical model. Indeed, in this case, residence time of the fluid in the tank decreases as well as heat losses. The authors proved that the stabilized cycle is not affected by one-time disruption and by temperature level if the thermo-physical properties of the fluid remain in the same order of magnitude. The same observations were made by Zarrinehkafsh & Sadrameli [24] with numerical simulations. However, their experiments involved a mass flow rate between $0.01\text{kg} \cdot \text{s}^{-1}$ and $0.015\text{kg} \cdot \text{s}^{-1}$ which is too small to reveal significant performance differences. In a vertical TES, raising flow rate reduced heat losses during charging and discharging time and buoyancy forces due to flow inertia. The same observation was demonstrated on a horizontal geometry prototype [25]. Hoffmann *et al.* [26] noticed the existence of an optimal flow rate for which the discharge efficiency is maximum. Below this value, heat losses increase as well as thermal diffusion. Above this value, forced advection is major, because heat exchange between fluid and solid particles is too weak. Another observation showed that by increasing the particle diameter, the optimal flow rate is lower. The same idea was resumed by Esence *et al.* [27], who defined the optimal velocity as a trade-off mainly between heat losses and stratification. Their numerical model showed that the lower the heat loss coefficient, the lower the optimal velocity. As a result the utilization rate, which is the ratio between energy discharged and theoretical storage capacity, increases. Despite the existence of an optimal velocity, Vannerem *et al.* [28] could not find it with their prototype because the fluid velocity effect was too moderate. Indeed, they reported that velocity and temperature have less influence on storage performance. Consequently, their packed-bed storage is robust to these variations. Moradi *et al.* [29] studied the influence of charging air velocity for different fillers (alumina, silica and metal). Lower air velocities improved the storage efficiency.

Other operating conditions have been investigated such as charging and threshold temperatures. Fasquelle *et al.* [30] noted that the use of a dynamic threshold temperature is an appropriate strategy for a TES interconnected to a Concentrated Solar Power (CSP) plant. Moradi *et al.* [29] supplemented their study with an investigation into the influence of charging air temperature. The results indicated that the recovery efficiency is better for higher inlet air temperature. Lopez-Ferber *et al.* [31] studied the influence of degraded operating conditions, such as the temperature and flow rate on an horizontal packed-bed prototype. They showed that degraded inlet temperatures and flow rates do not have significant effects on the load ratio, obtained by dividing the energy stored by the maximum energy that the TES can store. As a result, the thermocline prototype was able to handle degraded heat fields. Moreover, increasing the threshold discharging temperature results in a reduction in storage efficiency and an improvement in the power output. Whereas, the storage yield increases with the threshold charging temperature. The prototype used by the authors was then scaled-up to an industrial size. The industrial-scale packed-bed TES has been described and studied by Touzo *et al.* [20] in previous work. To simulate the effect of solar heat sources on this storage, Touzo *et al.* [32, 33] simulated solar power variation along the day and also intermittencies, due to potential clouds. The first test has a minor impact on the thermocline TES. As for the second test, the stand-by processes significantly reduced the storage yield, due to heat losses and

both radial and axial stratification.

The studies presented in this literature review do not systematically compare a numerical model with a prototype, with variations in operating conditions. Moreover, the few prototypes studied are generally of low capacity and small size [22–26, 28–31]. Some studies seek to validate numerical models from experimental data [23,24,29]. Only five studies investigated the influence of the temperature and/or flow rate variations on the storage performance [26, 28–31]. However, these systems are at the laboratory scale, which is not very representative of the larger scale applications. Some industrial-scale packed-bed TES have been manufactured and studied. The best known are the Solar One [34] and Pacheco *et al.* [35] thermocline tanks. Recently, other industrial-scale packed-bed storage systems have been constructed. The Ait Baha CSP plant in Morocco has been equipped with a 100 MWh_{th} thermocline storage composed by rock particles [36]. A prototype of horizontal storage composed of hollow bricks has also been built [37,38]. However, to the best of our knowledge no studies have been performed on the ability of industrial-scale packed-bed storage systems to operate under degraded conditions. Moreover, these articles do not take into account the evolution of the characteristic time of the variations in operating conditions.

Knowing the influence of operating conditions on some laboratory-scale packed-bed storage systems, the same phenomena must be investigated on an industrial-scale thermocline TES. This study focuses on the thermocline TES described by Touzo *et al.* [20] which seeks to recover waste heat. Indeed, the valorization of industrial waste heat is characterized by the strongest disparity of fields, both in temperature and in flow rate, which complicates the recovery of industrial heat. To be effective, a TES must be able to transform a variable field into a controlled source of heat. The scope of this study is to examine the influence of two operating conditions (temperature and flow rate) of the industrial-scale high-temperature air/ceramic horizontal thermocline TES, commercialized by Eco-Tech Ceram. For this purpose, long and short characteristic times as well as sudden or gradual temperature and flow rate changes are analyzed to simulate real waste heat fields and to determine storage efficiency. The article is organized as follows. In the first part (see section 2), the methodology is described, including the experimental setup, the numerical model and storage performance indicators. In the second part (see section 3), the results are presented into three sections. First, charging temperature changes are studied under three scenarios: sudden temperature change, longer or shorter periods and gradual temperature change. Then, charging and discharging flow rates are modified with the same scheme: sudden, temporal and progressive changes. Since the flow rate has a direct influence on the storage performance, a complementary section aims to demonstrate the difference between the two operating conditions (temperature and flow rate), showing the existence of an optimal flow rate. Finally, the combination of temperature and flow rate variations is investigated through a typical industrial ceramic manufacturing process. The last part concludes (see section 4).

2 Materials and methods

2.1 Experimental setup

The experimental setup, describe by Touzo *et al.* [20], consists of three main elements: an electrical cabinet, an air heater skid and a thermocline TES, called Eco-Stock®, as illustrated in Figure 2a. The air skid is composed by the air admission, a fan, an electric air heater (500 kW_e), a chimney and a set of valves. The experience consists of two steps: charging and discharging processes, shown in Figure 2b. During the charging step, ambient air enters through the air inlet, via a fan. Before passing through the TES, the air is heated in an electric air heater. Then, the cold air is sent to the chimney. For the discharging step, the direction of the HTF is reversed by valves (V1, V2, V3, V4 and V5). The ambient air is directly injected into the TES and the hot air is extracted.

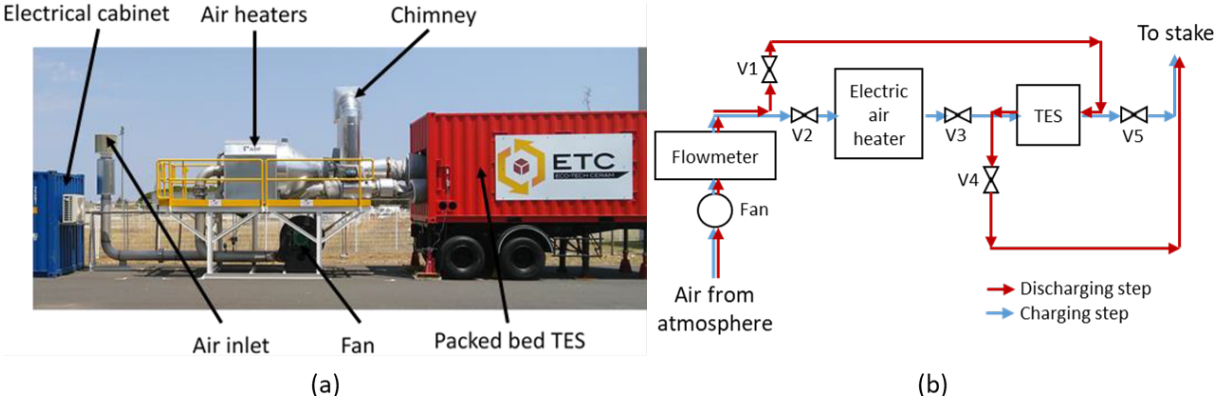

Figure 2: Commented picture of the experimental setup (a) and Schematic diagram of charging (blue) and discharging (red) processes

The storage under consideration is an industrial-scale air-ceramic horizontal packed-bed TES, commercialized by Eco-Tech Ceram (the container in red in Figure 2a). The inlet tank dimensions are 3.08 x 1.7 x 1.7 m^3. Its

specifications are shown in Table 1. This storage can store up to 1.9 MWh_{th} at 525°C (charged at 300 kW_{th}, discharged at 350 kW_{th}), as reported by Touzo *et al.* [20].

Table 1: Parameters of the industrial Eco-Stock® thermocline tank

Parameters of the tank	**Values**
Max hot temperature	600°C
Low temperature - ambient air	15 to 20°C
Mass of bauxite media	16 tons
Solid media diameter	30 mm
Total mass of the storage	28 tons
Porosity of the packed-bed	40%

A thermocline TES consists of a single tank. When the heat transfer fluid is injected into this tank, three different zones appear. Two quasi-uniform temperatures zones surround a zone with a large gradient. To follow the thermal behavior of the experimental TES, 33 K-thermocouples (accuracy +/- 2.2°C) are placed along the tank. Nine thermocouples track the temperature along a cross section at the beginning, middle and end of the tank [20]. These 9 thermocouples positioned along the storage are used to obtain the temperature profile, as shown in Figure 3. The flow rate is measured with a flowmeter placed at the fan outlet (see Figure 2b). The accuracy of the flowmeter used is 1.5 %.

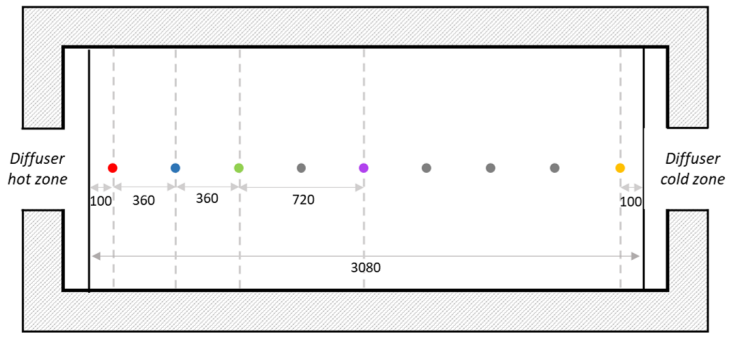

Figure 3: Position of the nine thermocouples along the tank

2.2 Numerical model

The physical model has been detailed in previous work [20]. The thermocline storage is modeled as a porous medium by a one-dimensional (radial gradients are neglected) and three-phase (heat transfer fluid, filler material and wall) model. The thermal phenomena due to conduction, convection, radiation and effective conductivity are determined. The temperature of the filler material is assumed to be homogeneous since the Biot number is calculated to be less than 0.1. All correlations used to estimate the heat transfer coefficients come from the work of Esence *et al.* [39].

Three energy equations are used: one describing the thermal behavior of the fluid (see eq 1), one of the solid (see eq 2) and one of the wall (see eq 3) [26,40]. Each equation has an accumulation term, a conduction term and a convection term. To model advection, an additional term is added to the fluid equation.

$$\varepsilon(\rho c_p)_{air}\left(\frac{\partial T_{air}}{\partial t}+u\frac{\partial T_{air}}{\partial x}\right)=\frac{\partial}{\partial x}\left(k_{air-eff}\frac{\partial T_{air}}{\partial x}\right)+h_v\left(T_{bau}-T_{air}\right)+h_w\frac{A_{air\leftrightarrow w}}{V_{air}+V_{bau}}(T_w-T_{air}) \quad (1)$$

$$(1-\varepsilon)(\rho c_p)_{bau}\frac{\partial T_{bau}}{\partial t}=\frac{\partial}{\partial x}\left(k_{bau-eff}\frac{\partial T_{bau}}{\partial x}\right)+h_v\left(T_{air}-T_{bau}\right) \quad (2)$$

$$(\rho c_p)_w\frac{\partial T_w}{\partial t}=\frac{\partial}{\partial x}\left(k_w\frac{\partial T_w}{\partial x}\right)+h_w\frac{A_{air\leftrightarrow w}}{V_w}\left(T_{air}-T_w\right)+h_{ext}\frac{A_{air\leftrightarrow ext}}{V_w}\left(T_{ext}-T_w\right) \quad (3)$$

with $k_{air-eff}$ and $k_{bau-eff}$ the effective conductivities of the fluid and the solid respectively, and h_v, h_w and h_{ext} the heat transfer coefficients.

The boundary conditions are an imposed temperature at the fluid inlet and an adiabatic condition at the fluid outlet. These equations are discretized by implicit finite difference. The applied discretization scheme is centered for the second order derivative and backward for the first order derivative.

This model has been validated at 525°C and 200 Nm^3/h for charging and discharging processes with the same industrial TES (Eco-Stock®). The deviation of the model is below 20°C for the temperature profiles.

2.3 Indicators

To determine the storage performance according to the temperature or flow rate variations, two different indicators are used, as defined in [20]. The first, called load ratio, is the amount of energy stored relative to the energy stored if the entire material was at the hot temperature.

$$\tau(t) = \frac{Q_{bau}(t)}{Q_{bau-max}} \tag{4}$$

The second indicator, called the local storage yield, is the ratio of energy discharged by the energy charged in the storage:

$$\gamma(t) = \frac{Q_{exc-d}(t)}{Q_{air-c}(t_{end-ch})} \tag{5}$$

Another indicator is used to show the relative temperature difference between the different temperature tests.

$$\Delta T_{relative} = \frac{(T - T_{ref})}{T_{ref}} \tag{6}$$

3 Results and discussion

The ability of the TES to absorb such temperature or flow rate variations is analyzed in this paper. To determine the effectiveness of the TES to transform these variations into a controlled source of heat, different parameters are investigated, as illustrated in Figure 4. The temperature (or flow rate) variations can be brutal (form of slots) and on the order of several hundred degrees (or $kg \cdot s^{-1}$). A slot can be described by its temperature (or flow rate) amplitude and its characteristic time. These parameters are studied to determine the capacity of the TES to smooth real waste heat field, as shown in the examples in Figure 1. The temperature amplitude has been studied by some authors [30,31]. However, no one has studied the characteristic time, which is very important in waste heat fields. Indeed, in such field, the same patterns are often found: sudden variations in flow rate (e.g. on flares), or flow rate ramps (e.g. on ceramic batch furnaces).

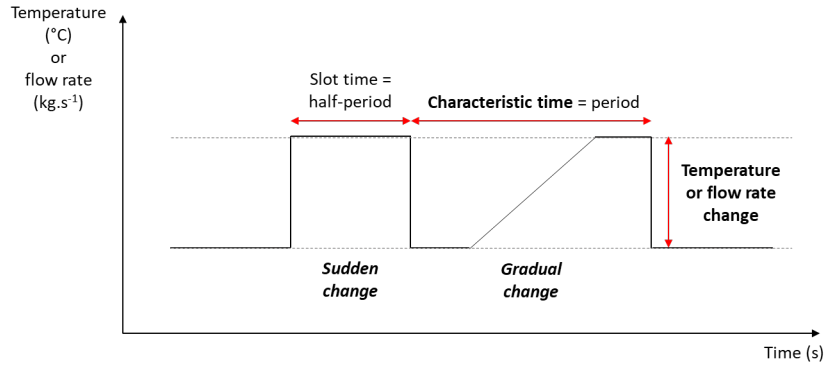

Figure 4: Diagram of the slot pattern of the waste heat field

The first part of the result section investigates the temperature variations. First, the sudden temperature change on the storage performance is studied. Longer and shorter characteristic times are analyzed. Finally, the influence of gradual temperature change on the TES efficiency is observed. The flow rate variations is studied in the second part, with the same scheme: sudden, temporal and gradual change. Finally, the difference between temperature and flow rate is shown, with the existence of an optimal flow rate.

3.1 Influence of temperature variation on performance

Before analyzing the influence of degraded temperature field on the storage performance, the cycling regime of the reference tank must be defined. This thermocline TES has been studied in a previous paper. Touzo *et al.* investigated the thermal behavior of three consecutive charge/discharge cycles at an inlet temperature of 525°C. Because of the hot air cannons which diffuse the air into the tank, in the charging process, the air flow rate was set to 0.58 $kg \cdot s^{-1}$ while in the discharging process it was 0.65 $kg \cdot s^{-1}$. To summarize, the thermocline TES was able to recover up to 90% of the heat source with a threshold discharging temperature of 200°C. The load ratio amounts to 62% for the third cycle. Considering a single charge/discharge cycle, the global storage yield was 83.4% [20].

This section details the results obtained by varying the charging temperature, with constant flow rates (0.58 $kg \cdot s^{-1}$ during charging process and 0.65 $kg \cdot s^{-1}$ during discharging process). The working conditions are summarized in Table 2.

Table 2: Summary table of tests

	Experiment	**Numerical model**	**Temperature (°C)**	**Load flow rate** ($kg \cdot s^{-1}$)	**Discharge flow rate** ($kg \cdot s^{-1}$)	**Slot time (h)**
Temperature robustness	X	X	320 to 500	0.58	0.65	0.5
	-	X	225 to 825	0.58	0.65	0.5
	-	X	320 to 500	0.58	0.65	0.25
	X	X	320 to 500	0.58	0.65	1.5
	X	X	100 to 520	0.58	0.65	-
Flow rate robustness	X	X	525	0.58	1.29	-
	X	X	500	0.29 to 0.58	0.65	0.5
	X	X	500	0.14 to 0.58	0.65	-
Robustness to operating conditions	X	X	50 to 500	0.37 to 0.58	0.65	-

3.1.1 Sensitivity to sudden temperature change

In order to analyze the sensitivity of the TES to sudden temperature changes, two tests were performed. The first one consisted of varying the charging temperature between 320°C and 500°C every 30 minutes, until the charging process was completed, as illustrated in Figure 5. The threshold charging temperature was set at 190°C. The flow rates are fixed at 0.58 $kg \cdot s^{-1}$ and 0.65 $kg \cdot s^{-1}$ respectively for the charging and discharging processes. This test is compared to an experimental reference load at a constant charging temperature of 410°C, i.e. the average of 320 and 500°C.

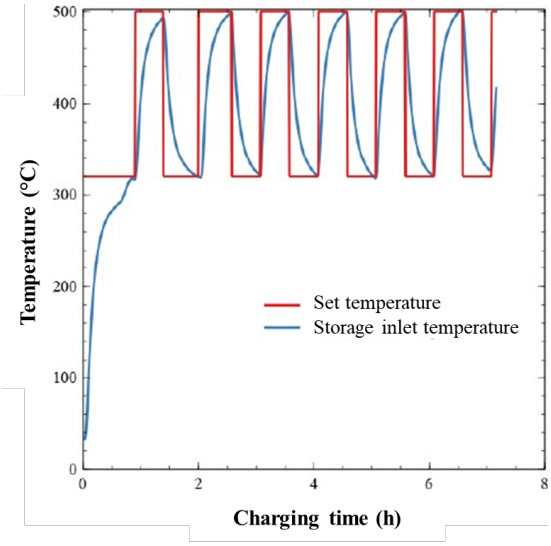

Figure 5: Evolution of the temperature, from 320 to 500°C, during the charging step of the 30 minutes slot test (charging flow rate of 0.58 $kg \cdot s^{-1}$)

Figure 6 shows the temperature profiles across the thermocline tank for the 30 minutes temperature slot test, from 320 to 500°C. For each curve, the abscissa (in mm) of the corresponding thermocouples (see Figure 3) is shown. The same color code is kept between the two charts (Figures 3 and 6). For the first thermocouple, located at 100 mm from the ceramic packed-bed (in red), the temperature oscillates by 50°C, around an average value of 410°C. This is small compared to the temperature variations injected into the system, from 320 to 500°C.

Consequently, the amplitude of the inlet temperature variations is divided by 4 after only 100 mm of ceramic packed-bed. After 460 mm of bed, the variations are very strongly absorbed. For this position, the temperature of the thermocouple oscillates only a few degrees around the average inlet temperature (410°C). A small layer of packed-bed acts as a thermal buffer on the heat field. Therefore, the thermocline storage shows a very satisfactory robustness against temperature variations. The numerical model is very accurate with an error of less than 2%, which is of the same order of magnitude as the measurement error.

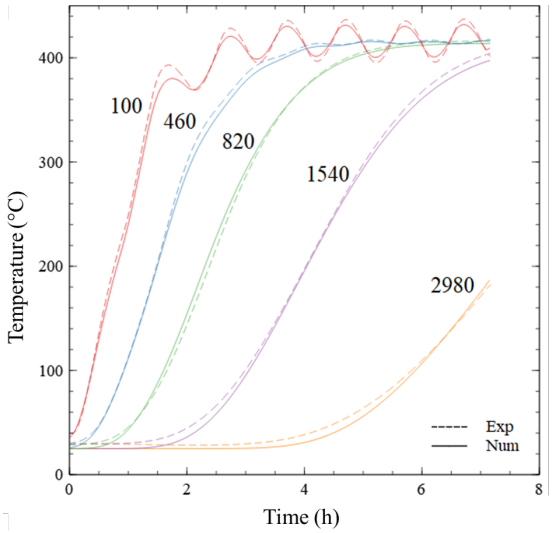

Figure 6: Evolution of the temperature of the thermocouples positioned in the flow axis of the TES (value corresponding to the position of each thermocouple in millimeters)

Figure 7a shows the experimental and numerical temperature profiles every two hours until the end of the test. The charging temperature of 320°C and 500°C are converted to a temperature step of 410°C. As a result, the TES is able to store a resource with a variable temperature by releasing it at a uniform temperature, which is the average field temperature. The length of the thermocline is about 1.5 m, which is the same as for the 525°C reference test. Therefore, the thermocline zone is apparently unaffected as is the thermal stratification.

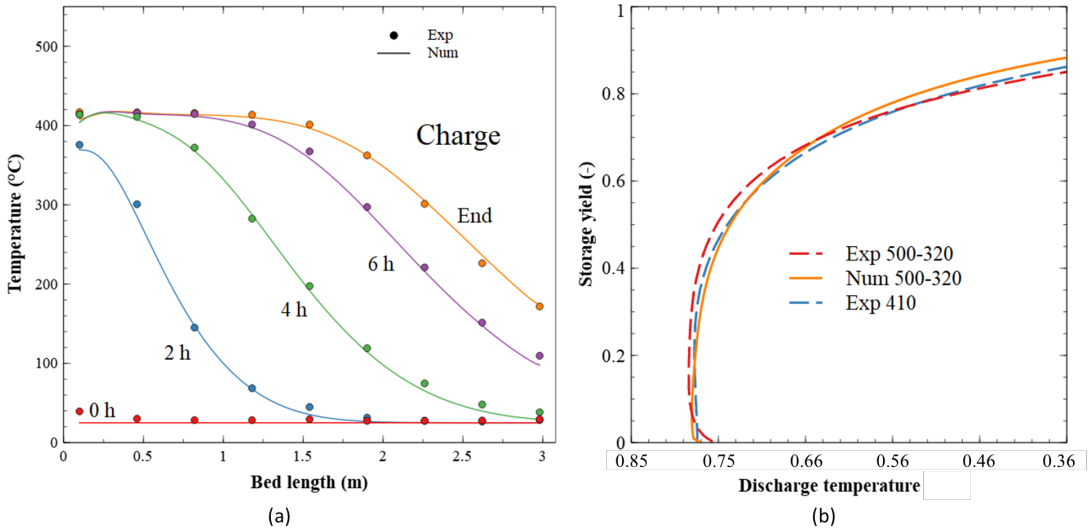

Figure 7: Temperature profiles (a) and local storage yield (b) of the test with charging temperature between 320 and 500°C alternating every 30 minutes

Figure 7b illustrates the experimental, numerical and reference local storage yields as function of unit temperature. For each scenario, over 40% of the energy is released at a constant temperature of 410°C (dimensionless temperature of 0.77). The output temperature then decreases, which is due to the extraction of the thermocline from the tank. Both tests have an identical behavior, proving the capacity of the TES to absorb the variation of the charging temperature without affecting its efficiency. The local storage yield is 76% for a valorized temperature of 300°C (dimensionless temperature of 0.56). For a dimensionless temperature of 0.36 (200°C),

it reaches 85%. Consequently, the yield is very dependent on the recovery temperature that the downstream energy process allows. Initially, the yield is slightly underestimated by the numerical model. In reality, it is only a question of representation: the efficiency is very sensitive to the discharging temperature at the beginning of the test [33]. Indeed, the yield is very sensible to high temperatures, as it varies from 0 to 40% for the same discharging temperature (see Figure 7b). On the other hand, the numerical model overestimates the efficiency by 3% for low discharging temperatures, which is the same error as in the reference case (temperature of 525°C). This error could be explained by temperature measurement errors during the experiment. The experimental unit and the numerical model show a very satisfactory robustness towards the temperature variation. As a result, the thermocline TES is able to smooth an oscillating temperature signal at its average temperature, as a thermal buffer.

A second test is performed to consider a larger temperature range of 500°C, from 225°C to 825°C. This modeling can be compared to the reference case realized at 525°C. The field then has a higher stress, which could further degrade the thermal front characterized by the end-of-charge profile (see Figure 8a). As shown by the relative temperature difference indicator (see Figure 8b), the temperature profiles are identical from 0.75 m of bed, with less than 0.5% error between 0.75 and 3 m of bed. The thermocline occupies 1.75 m of bed. The hot-side curve drops to about 400°C because the charging process ended at 225°C. Even with a 500°C variation, the TES appears to be able to absorb the temperature variation down to the average field temperature. The stratification of the thermocline was not affected. As a result, the ability of the thermocline TES to absorb the temperature variations seems to be independent of temperature range.

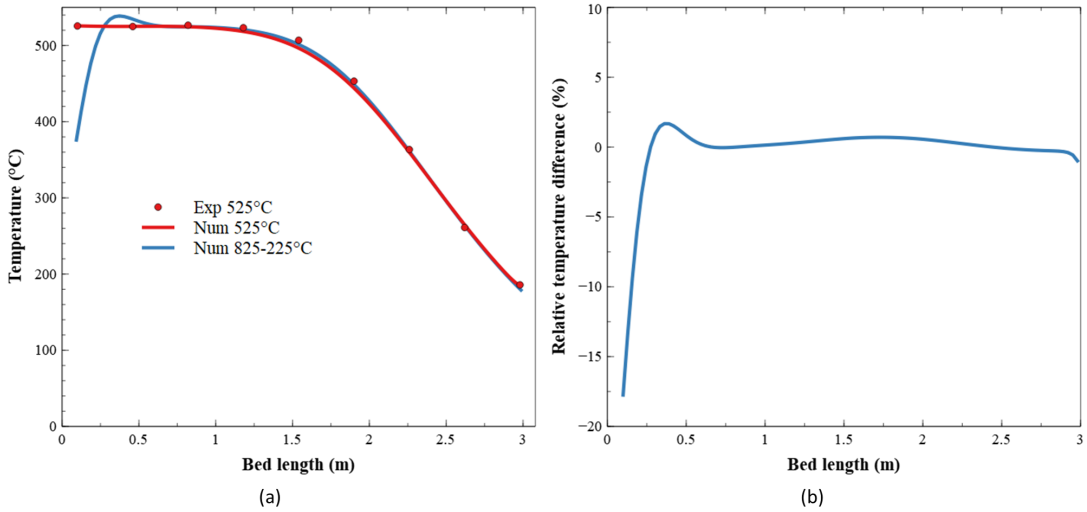

Figure 8: Comparison of end-of-charge profiles (a) and relative temperature difference (b) for temperature variations of 225-825°C

3.1.2 Sensitivity to the variation of the characteristic time

Since the influence of temperature range was studied in the previous section, the variation of the characteristic time, as depicted in Figure 4, can be analyzed. Three simulations were carried out with characteristic times of 15 minutes, 30 minutes and 1.5h. Figure 9 shows the end-of-charge temperature profiles for 15 and 30 minutes slot times (a), along with the relative temperature difference between these tests and the reference case (b). The two end-of-charge profiles are perfectly identical (less than 2.5% error into the thermocline zone), except on the hot side. In the 15 minutes slot time case, 30 cm of storage is required to filter the signal, while about 60 cm is needed for the 30 minutes slot time, as illustrated with the relative difference temperature. Consequently, a decrease in the characteristic time would have no impact on the storage performance. With a slot time of 1.5h presented in Figure 10, a disturbance in the end-of-charge profile is observed (between 1 and 2 m of bed). The thermal stratification is disturbed and the plateau classically observed in the case of a thermocline TES does not appear anymore. As a result, the three zones are no longer distinct. The TES can no longer discharge its heat at a constant temperature, but in a high temperature range. An equivalent experiment on the storage unit was also performed.

As the storage heat front is less stratified, the performance of the thermocline TES may be altered. Figure 10 shows that the discharging temperature starts at 350°C (dimensionless temperature of 0.66) for the 1.5h slot time (1.5h test) against 400°C (dimensionless temperature of 0.75) for the 0.5h slot time (0.5h test). The discharging temperature then increases to a dimensionless temperature of 0.79 (420°C) before decreasing. The discharging start temperature is relatively low, which can be problematic. Indeed, if the downstream process defines for example a threshold temperature of 380°C (dimensionless temperature of 0.72), the beginning of the

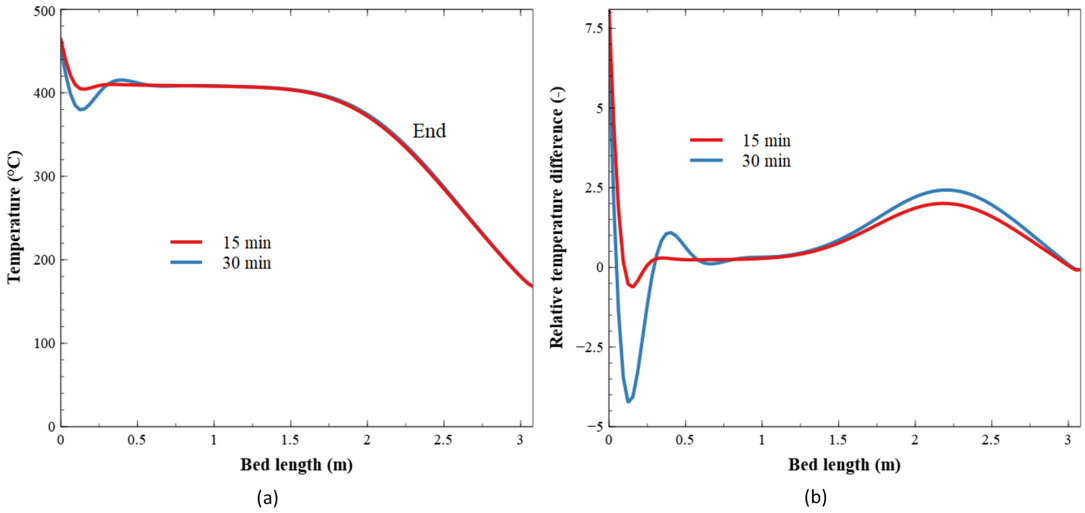

Figure 9: Comparison of end-of-charge profiles (a) and relative temperature difference (b) for temperature variations of 320-500°C every 15 minutes and 30 minutes

storage discharge cannot be valorized and must be evacuated by the chimney. Consequently, the TES is no longer available to release the stored heat to a constant temperature. The 0.5h test allows 40% of the heat to be restored at a dimensionless temperature of 0.77 (410°C), compared to 17% for the 1.5h test. However, with lower threshold temperatures, below 350°C (dimensionless temperature of 0.66), the performance of the two scenarios converge. Local storage yields of 66%, 76% and 82% are achieved for threshold dimensionless discharging temperatures of 0.66, 0.56 and 0.46 respectively.

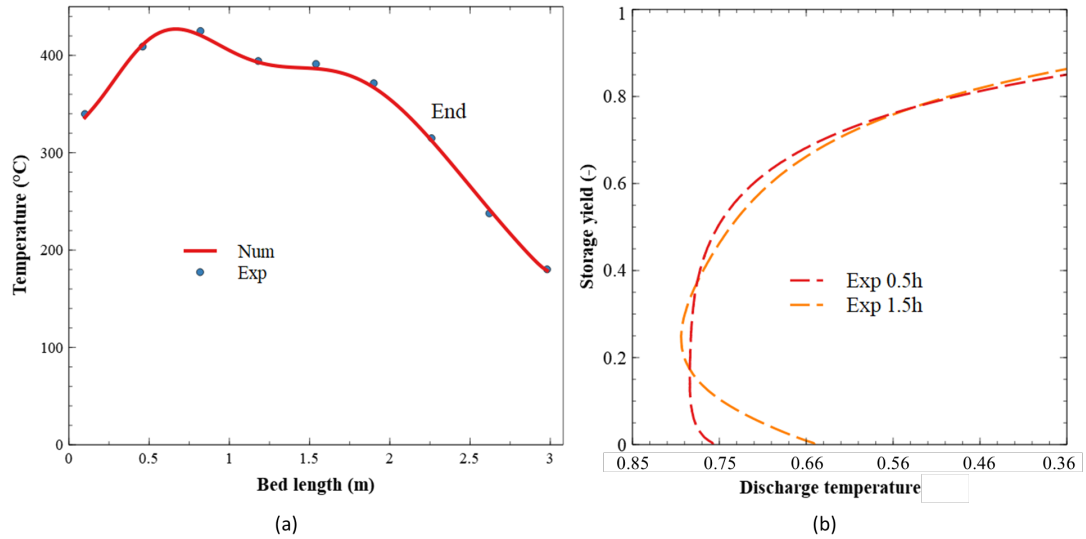

Figure 10: End-of-charge profiles (a) and local storage yield (b) for temperature variations of 320-500°C every 1.5h

We were interested in the ratio of the stored energy to the advected power, i.e. the product of the non-dimensional Biot and Fourier numbers. The values obtained are 3.6, 7.2 and 21.6 respectively for slot times of 0.25, 0.5 and 1.5 h. According to the results obtained in this section, the Eco-Stock® is able to absorb temperature variations for a Biot and Fourier product of less than 20. Above this value, the Eco-Stock® is no longer able to release all the stored heat.

3.1.3 Sensitivity to gradual temperature change

Some waste heat fields are composed by a gradual temperature change. Another test is carried out with increasing charging temperature: from 100°C to 520°C, from 0h to 7h of the charging process, and the temperature is maintained constant until the end of the charging process at 7.4h. The threshold charging temperature was set at

170°C. Figure 11a illustrates the temperature profiles every 2h. These profiles appear as parallel lines within the storage. Indeed, the material located at the inlet of the tank rises in temperature and progressively approaches the charging temperature. However, with increasing temperature variation throughout test, the material never reaches the charging temperature. As a result, the threshold charging temperature is reached without any uniform temperature zone being created.

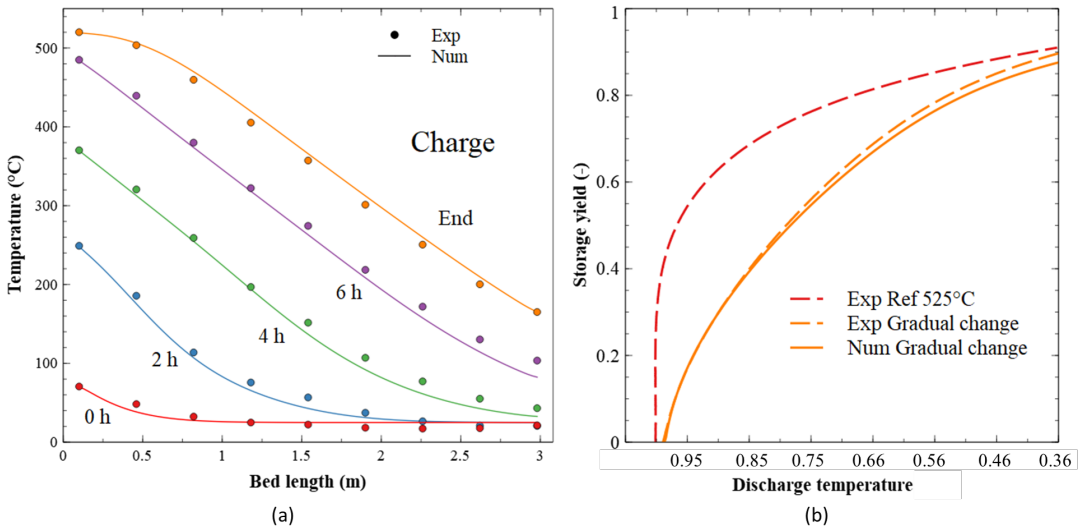

Figure 11: Temperature profiles (a) and local storage yield (b) of the gradual temperature change from 100°C to 520°C

To measure the degradation of stratification, the local storage yield is determined (see Figure 11b). Unlike the reference case (constant charging temperature of 525°C), the TES was not able to restore heat at constant temperature. Indeed, the temperature decreases almost linearly to reach an efficiency of 40% for a dimensionless discharging temperature of 0.85, which is 25% lower than the reference test. Consequently, the local storage yield is strongly affected by the gradual temperature change. The numerical model is less accurate for this test. An increasing deviation from the experimental results is observed, until reaching a difference of 4% at 200°C (dimensionless temperature of 0.36). This deviation is due to the initial state of the TES, which was not at ambient temperature. Therefore, a radial perturbation is visible in the tank. However, it is not possible to account radial temperature heterogeneity in a one-dimensional model.

The results of this section show that the storage performance remains stable and comparable to the average temperature of the heat field as long as the characteristic time of the temperature variations is significantly shorter than that of the charging and discharging process.

3.2 Influence of flow rate variation on performance

Knowing the behavior of the thermocline TES when the heat field exhibits temperature variations, the influence of the flow rate variations on the storage performance is studied. In this section, different charging scenarios are compared. The first scenario is a reference test, with a constant air flow rate and a constant charging temperature. In the second scenario, the influence of a high discharge flow rate is studied. The last two scenarios investigate the evolution of the load flow rate: one scenario deals with a sudden change in flow rate and the other with a gradual increase in flow rate. The working conditions are summarized in Table 2.

3.2.1 Sensitivity to high discharge flow rate

This test is performed with a discharge flow rate of 1.29 $kg \cdot s^{-1}$. The discharging temperature profiles at 0h, 1h, 2h and 2h57 are illustrated in Figure 12a. For the reference case (discharge flow rate of 0.65 $kg \cdot s^{-1}$), the discharging temperature profiles are shown for 0h, 2h, 4h and 5h56 to correspond to the same energy released as the high flow rate test. The discharge time was divided by 2.01 between the reference (5h56) and the high flow rate (2h57) tests. Consequently, the TES has no limitations in terms of heat exchange over this flow range. Moreover, thermal stratification does not appear to be affected by higher flow rates. A constant temperature difference, not exceeding 20°C, is observed between the two experimental tests. Although the reference temperature profiles are a few degrees higher during discharging process, the opposite occurs in the end-of-discharge profile. This could be due to a better stratification of the reference test, allowing a higher discharge of the storage for the same threshold discharging temperature.

Numerical and experimental storage yields are plotted for both scenarios (see Figure 12b). All three yields show similar trends, with a constant temperature at 525°C (dimensionless temperature of 1) until the yield

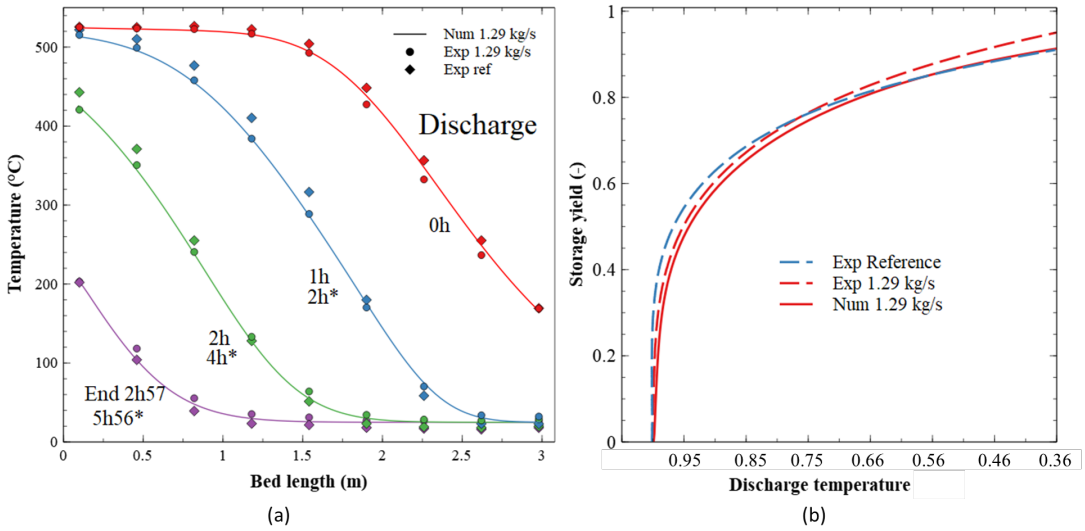

Figure 12: Temperature profiles (a) and local storage yield (b) of the high flow rate test

reaches 30%. The discharging temperature then decreases, most strongly for the 1.29 kg $\cdot$ s^{-1} test. The maximum difference is 4% between the two experimental curves, reached for a dimensionless temperature of 0.95. However, this difference then decreases for lower discharging temperatures. The stratification that seemed slightly better for the reference case is observed here. Indeed, more energy can be discharged at 525°C. The numerical modeling accurately represents the performance, with a maximum gap of 4%.

To sum up, the storage performance appears to be nearly identical for these two scenarios. Doubling the discharge flow rate does not affect the storage performance. Lopez-Ferber *et al.* made the same observation on their prototype [31]. The flow rate had been doubled and tripled without observing any variation in performance. This result is now confirmed on an industrial unit.

3.2.2 Sensitivity to the variation of the characteristic time

In a second test, the charging flow rate varies from 0.29 kg $\cdot$ s^{-1} to 0.58 kg $\cdot$ s^{-1} every 30 minutes (slot test). The threshold charging temperature was set at 180°C. A check of the flow rate measured by flow meter showed that the flow rate follows the set flow rate, as illustrated in Figure 13. Consequently, the fan control adapts to the set point in less than one minute.

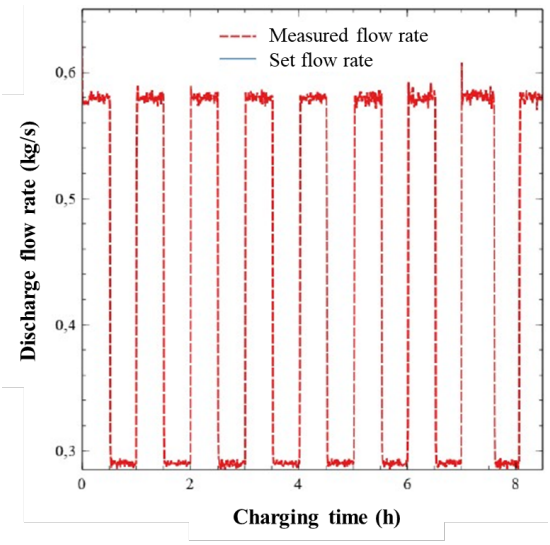

Figure 13: Evolution of fan flow rate, from 0.29 to 0.58 kg $\cdot$ s^{-1}, during the charging step of the 30 minutes slot test (charging temperature of 500°C)

The temperature profiles are illustrated in Figure 14a. The experimental reference case is plotted for 0h, 1h30, 3h, 4h30, 6h and at the end of the charging process, so as to obtain a charging energy similar to the slot

test. The discharge flow rate of the reference case is 0.65 $kg \cdot s^{-1}$. The experimental and numerical profiles are superimposed. Therefore, the model tolerates sudden variations in flow rate without affecting its accuracy. At the end of the charging process, the profiles of the reference and the slot test are identical. The thermocline zone occupies 1.5 m of the bed. As a result, the flow rate variations did not affect the thermal stratification.

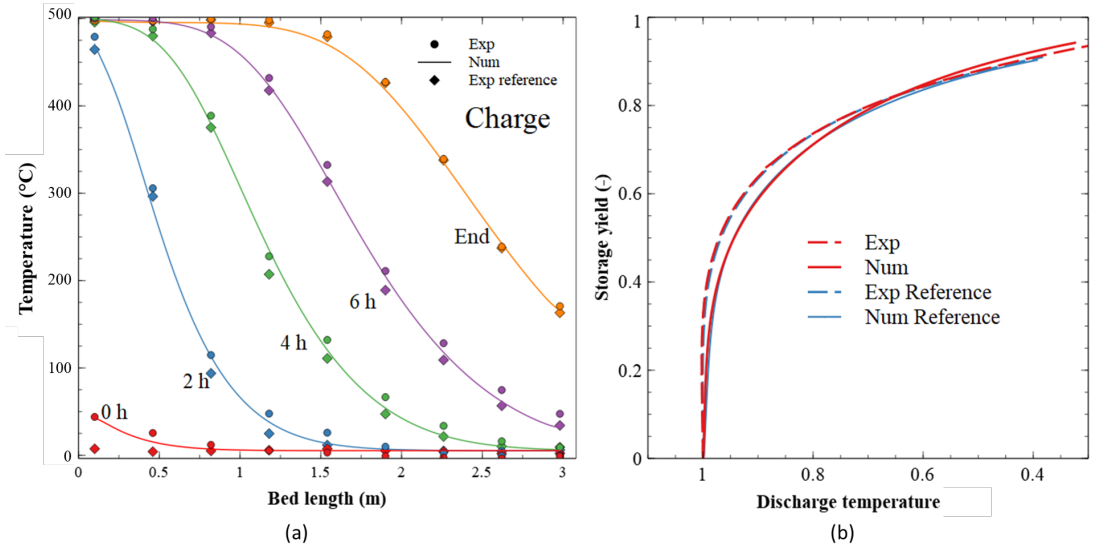

Figure 14: Temperature profiles (a) and local storage yield (b) of the slot test

The yield is also studied to verify that the constraint applied to the flow rate does not impact its performance. The experimental efficiencies merge for all discharging temperatures in Figure 14b. All scenarios achieve a yield of 0.4 at a relatively constant temperature before the temperature drops. The numerical model is again found to be reliable, with less than 4% difference from the experiment.

3.2.3 Sensitivity to gradual change in charging flow rate

Some waste heat fields are made up by gradually changing the charge flow rate. Another test is performed by increasing the charge flow rate from 0.14 $kg \cdot s^{-1}$ to 0.57 $kg \cdot s^{-1}$ from 0h to 4h of charging process. The test continues at a constant charge flow rate until the threshold temperature of 180°C is reached. The charging temperature profiles are shown in Figure 15a for 0h, 2h, 4h, 6h and at the end of the charging process. Thermal stratification does not appear to be affected by gradual change in charging flow rate, as illustrated with the temperature profiles of the reference case in [20]. Figure 15b shows the local storage yields of the gradual flow rate ramp test as a function of discharging temperature. For a temperature of 210°C (dimensionless temperature of 0.38), the storage yield is 88%. Note that the yields decrease with the reduction of the flow rate. The start of the charging step was performed at 0.14 $kg \cdot s^{-1}$. The forced convective exchanges are reduced while the heat loss and diffusion are favored. The thermocline zone increases which degrades the thermal performance. The numerical resolution is again good with less than 2.5% deviation from the experimental results. This model is thus validated from 0.14 $kg \cdot s^{-1}$ to 1.29 $kg \cdot s^{-1}$. The TES is adapted to several flow rates and so several types of heat field. The limit of 1.29 $kg \cdot s^{-1}$ could be exceeded with a more powerful fan. Therefore, the maximum discharging power of the Eco-Stock® is likely to be much higher than the results presented here.

The gradual change in charging flow rate suggests that decreasing the flow rate too much affects the storage performance. As a result, it would appear that there is an optimal operating point or range for the TES.

3.2.4 Optimal flow rate

In order to target the most suitable fields for recovery, an optimal operating range is established. Some authors have shown that the tank performance increases with the fluid inlet speed until a limit is reached [27,28,41]. Figure 16 illustrates the sensitivity of the charging rate to the charging flow rate between 0.1 $kg \cdot s^{-1}$ and 1 $kg \cdot s^{-1}$. This performance indicator is chosen because it quantifies the destratification on a single thermocline displacement in the TES. The charging rate is 0.74 for a flow rate of 0.1 $kg \cdot s^{-1}$. Then it reaches 0.805 for a flow rate of 0.5 $kg \cdot s^{-1}$ and stabilizes at this value until 1 $kg \cdot s^{-1}$. This indicator is related to the thermocline. Consequently, the more stratified the thermocline, the more energy the TES can hold. The lower the flow rate, the longer the residence time of the fluid in the system. Therefore, thermal diffusion is more important than forced convection. Increasing the residence time of the fluid reduces stratification.

In this test, the existence of an optimal flow rate is not as well marked as in the case of liquid heat transfer systems. The optimal flow rate results from a compromise between the heat carried by the fluid along the bed

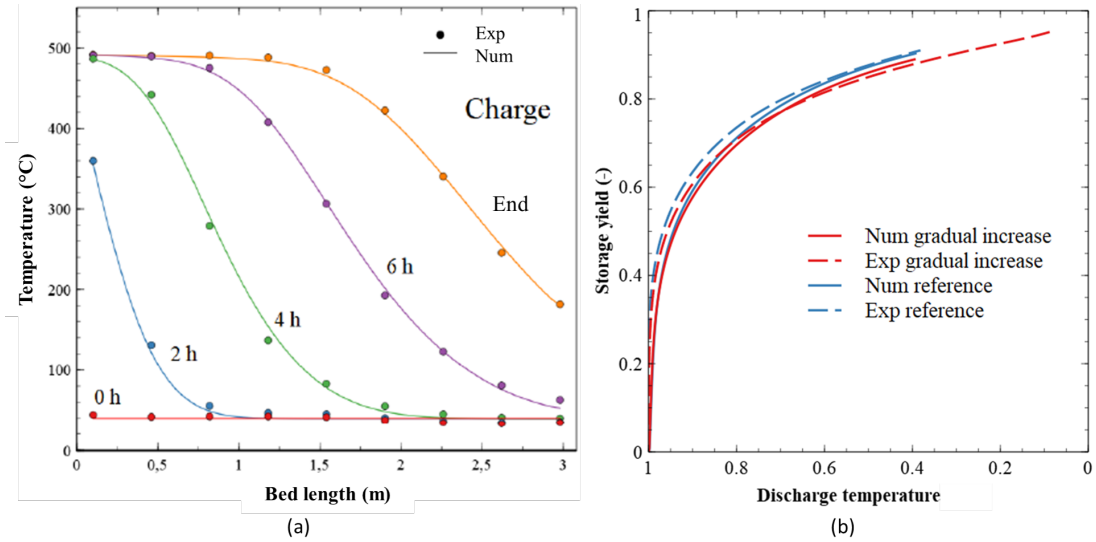

Figure 15: Temperature profiles (a) and local storage yield (b) of the flow rate ramp test, compared to numerical and reference local yields

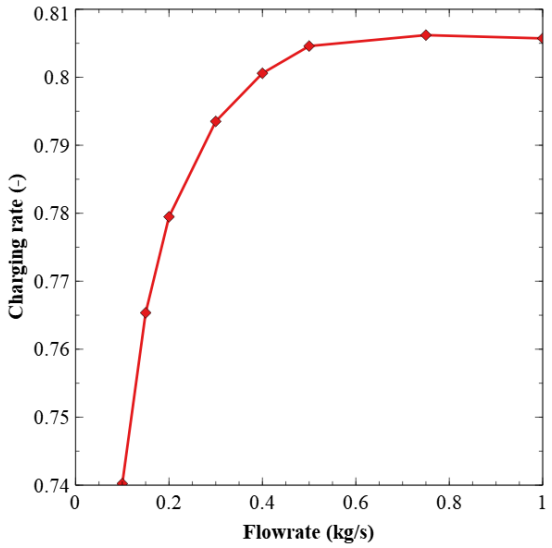

Figure 16: Charging rate as a function of charging flow rate from the numerical model

and the heat transferred to the solid. In the case of a heat transfer gas, the fluid carries little heat per unit volume because of its low density. Therefore, disproportionate speeds must be reached for advection to prevail over convection. Therefore, the drop in performance at high flow rates is gradual and delayed, and leads to a performance plateau. Very high flow rates are not studied in this work, to show the decrease of charging rate, because they are not possible in the considered industrial processes.

These observations are reflected in the various flow rate tests. Indeed, the storage performance is affected in the ramp test (0.14 $kg \cdot s^{-1}$ to 0.58 $kg \cdot s^{-1}$). The reference and high discharge flow rate tests are in the performance plateau. The slot test was performed before (0.14 $kg \cdot s^{-1}$) and on the performance plateau (0.58 $kg \cdot s^{-1}$). As a result, the average charge rate for these two operating points would lead to an average charge rate of 0.8, which is 0.5% below the performance plateau.

3.3 Case study of a ceramic process: influence of temperature and flow rate variations on performance

The respective influence of temperature and flow rate variations on thermocline storage performance has been observed separately in the previous sections. In waste heat fields, both variations can occur. Therefore, these two variations are coupled in this section. An experimental test representing the integration of the TES into an energy process chain is studied. A heat ceramic process, which captures and stores heat from fumes of a kiln, is investigated to determine the robustness of the storage to simultaneous temperature and flow rate variations. Figure 17 shows the temperature and flow rate fields of this heat from ceramic manufacturing process. The waste heat temperature increases from 100°C to 480°C during the first 4h of charging process, and the flow rate significantly fluctuates from 0.37 $kg \cdot s^{-1}$ to 0.58 $kg \cdot s^{-1}$.

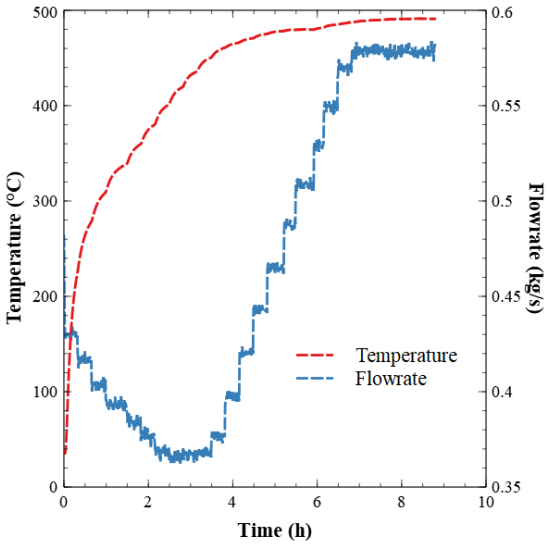

Figure 17: Heat from ceramic process

Figure 18a shows the temperature profiles obtained for the heat ceramic process. The thermocline thickens to 2 m compared to 1.5 m for the reference case. Therefore, thermal destratification is observed, probably due to the charging temperature ramp. Indeed, in this test, the thermocline zone occupied the whole tank. Under the conditions of the studied ceramic process (see Figure 17), the flow rate remains close to the performance plateau identified in Figure 16. As a result, the degradation of heat exchange seems to be caused mainly by temperature variations. The numerical model is reliable since the numerical temperature profiles coincide with the experimental points.

In order to quantify the performance decrease related to the observed destratification, the yield has been plotted in Figure 18b. Only 20% of the heat can be restored at the maximum charging temperature. Then, outlet temperature decreases sharply. For the same discharging temperature of 420°C (dimensionless temperature of 0.79), the yield is 73.5% for the reference case and only 68% for the ceramic test, i.e. a 5.5% yield loss. The heat ceramic process does not present ideal conditions for use of thermocline TES. Nevertheless, the TES is able to restore 88% of the heat field at a dimensionless temperature above 0.36. This is 3% less than the reference case (charging temperature of 525°C).

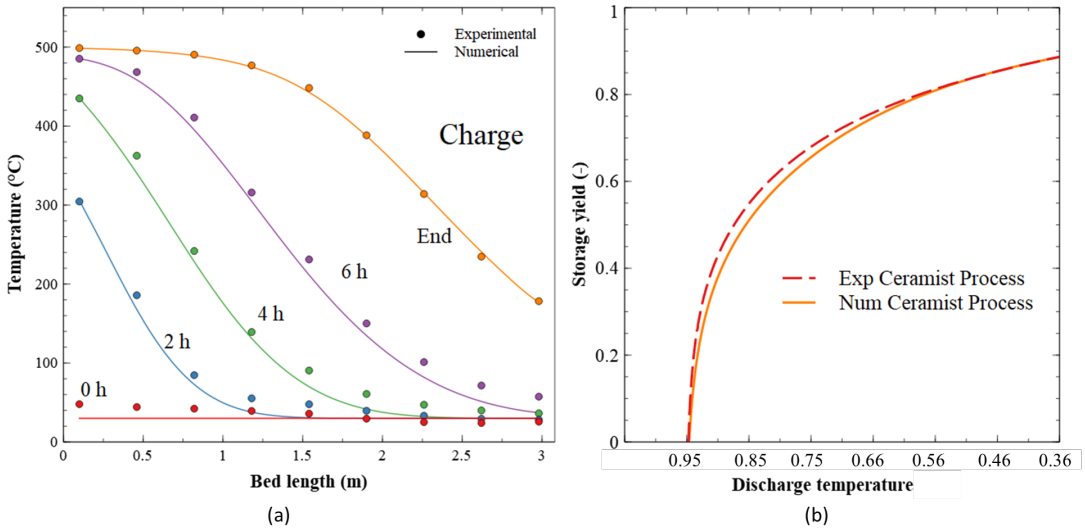

Figure 18: Temperature profiles (a) and local storage yield (b) of the heat from ceramic process

4 Conclusion

In this study, the experimental and numerical performance of an industrial-scale air-ceramic horizontal packed-bed TES is evaluated. To simulate the integration conditions of degraded waste heat fields, strong temperature and flow rate constraints were applied. The horizontal thermocline TES was tested with nine different cases to determine the storage robustness to individual or simultaneous temperature and flow rate variations. Simultaneous fluctuations in temperature and flow rate are obtained by individually varying these two operating conditions to represent a real waste heat field.

The numerical model has proven its robustness for non-uniform temperatures and flow rates during the charging process, as well as for operating regimes, with a maximum deviation of less than 4% for all scenarios. It is able to cope with large variations in its boundary conditions.

The results showed that this Eco-Stock® was extremely effective in storing a variation temperature heat field, except for gradual temperature changes, and releasing it with good performance indicators. For example, the local storage yield reached 66% at an outlet temperature of 350°C for all temperature tests. During charging temperature variations, the storage thermal inertia allowed the field to be smoothed to store and then release the heat at the average temperature of the heat field. However, increasing the characteristic time to a duration of the same order of magnitude as the charging time can decrease the quality of thermal stratification.

It was also found that degraded flow rate during the charging or discharging process had no effect on the local storage yield at 420°C. The yields are between 71% to 73.5% over the range of 0.14 $kg \cdot s^{-1}$ to 1.29 $kg \cdot s^{-1}$. Consequently, the Eco-Stock® is suitable for several flow rates and thus several field types. However, it is necessary to stay above a threshold flow rate because the lower the flow rate, the lower the yield seems to be. Below this threshold, forced convection decreases, heat diffusion and heat loss increase. The thermal destratification raises and so the storage performance decreases. Therefore, this work supports this observation which has already been highlighted in the literature [26, 27]. Moreover, the limit of 1.29 $kg \cdot s^{-1}$ in the discharging process could be exceeded with a more powerful fan. The maximum discharge power would probably be much higher in this case than the results presented in this study. As flow rate directly influences the storage performance, this study has shown that there is an optimal operating range. At a flow rate of 0.5 $kg \cdot s^{-1}$, the charging rate reaches 0.805.

Another test studied the impact of the two simultaneous variations on the thermocline TES. The Eco-Stock® was able to recover the waste heat from a field representative of a ceramic application. The yield is 5.5% lower than the reference case for a threshold discharging temperature of 420°C. Indeed, an increasing field temperature is one of the most unfavorable conditions for the charging process of a thermocline TES. Therefore, the Eco-Stock® has demonstrated its robustness for non-uniform temperatures and flow rates during the charging process, as well as for operating regimes. Consequently, it is able to manage degraded heat fields.

It would be also possible to use the Eco-Stock® coupled with gas burners to preheat the combustion air. The drop in outlet temperature can then be compensated and the downstream process can be fed at constant temperature. In addition, it would be possible to use some of the heat in high-temperature equipment and then use the low-temperature heat in dryer-type equipment, accepting lower temperatures. This application was carried out for the first industrial installation of Eco-Tech Ceram at the ceramist *Céramiques et Développement*[1].

[1] https ://www.ecotechceram.com/tegulys/

5 Acknowledgments

This project has received funding from the program "investissement d'avenir" (investments for future) of the "Agence Nationale de la Recherche" (National Agency for Research) of the French state under award number ANR-10-LBX-22-01-SOLSTICE, and from BPI France from the World Innovation Competition Phase 2 for the Eco-Stock® project.

6 References

References

[1] Hussam Jouhara and Abdul Ghani Olabi. Editorial: Industrial waste heat recovery. *Energy*, 160:1–2, October 2018.

[2] ADEME. *Excess heat*. Number 010559. ADEME, Angers, 2017 edition, April 2018.

[3] Gregoris P. Panayiotou, Giuseppe Bianchi, Giorgos Georgiou, Lazaros Aresti, Maria Argyrou, Rafaela Agathokleous, Konstantinos M. Tsamos, Savvas A. Tassou, Georgios Florides, Soteris Kalogirou, and Paul Christodoulides. Preliminary assessment of waste heat potential in major European industries. *Energy Procedia*, 123:335–345, September 2017.

[4] Ilona Johnson, William T. Choate, and Amber Davidson. Waste Heat Recovery. Technology and Opportunities in U.S. Industry. Technical report, BCS, Inc., Laurel, MD (United States), March 2008.

[5] United Nations. Adoption of the Paris Agreement. Technical Report FCCC/CP/2015/10/Add.1, United Nations, Paris, November 2015.

[6] Hussam Jouhara, Navid Khordehgah, Sulaiman Almahmoud, Bertrand Delpech, Amisha Chauhan, and Savvas A. Tassou. Waste heat recovery technologies and applications. *Thermal Science and Engineering Progress*, 6:268–289, June 2018.

[7] Veronika Wilk, Bernd Windholz, Reinhard Jentsch, Thomas Fleckl, Jürgen Fluch, Anna Grubbauer, Christoph Brunner, Daniel Lange, Dietrich Wertz, and Karl Ponweiser. Valorization of industrial waste heat by heat pumps based on case studies of the project EnPro. In *12th IEA Heat Pump Conference 2017*, page 10, Rotterdam, 2017.

[8] Bernardo Peris, Joaquín Navarro-Esbrí, Francisco Molés, and Adrián Mota-Babiloni. Experimental study of an ORC (organic Rankine cycle) for low grade waste heat recovery in a ceramic industry. *Energy*, 85:534–542, June 2015.

[9] Steven Lecompte, Oyeniyi A. Oyewunmi, Christos N. Markides, Marija Lazova, Alihan Kaya, Martijn Van den Broek, and Michel De Paepe. Case Study of an Organic Rankine Cycle (ORC) for Waste Heat Recovery from an Electric Arc Furnace (EAF). *Energies*, 10(5):649, May 2017. Number: 5 Publisher: Multidisciplinary Digital Publishing Institute.

[10] Arash Nemati, Hossein Nami, Faramarz Ranjbar, and Mortaza Yari. A comparative thermodynamic analysis of ORC and Kalina cycles for waste heat recovery: A case study for CGAM cogeneration system. *Case Studies in Thermal Engineering*, 9:1–13, March 2017.

[11] Mathilde Blaise and Michel Feidt. Waste Heat Recovery and Conversion into Electricity: Current Solutions and Assessment. *International Journal of Thermodynamics*, 22(1):1–7, March 2019. Number: 1.

[12] Terry Hendricks and William T. Choate. Engineering Scoping Study of Thermoelectric Generator Systems for Industrial Waste Heat Recovery. Technical report, Pacific Northwest National Lab. (PNNL), Richland, WA (United States), November 2006.

[13] Yiyu Men, Xiaohua Liu, and Tao Zhang. A review of boiler waste heat recovery technologies in the medium-low temperature range. *Energy*, 237:121560, December 2021.

[14] Laia Miró, Jaume Gasia, and Luisa F. Cabeza. Thermal energy storage (TES) for industrial waste heat (IWH) recovery: A review. *Applied Energy*, 179:284–301, October 2016.

[15] Giovanni Manente, Yulong Ding, and Adriano Sciacovelli. A structured procedure for the selection of thermal energy storage options for utilization and conversion of industrial waste heat. *Journal of Energy Storage*, 51:104411, July 2022.

[16] Doug Brosseau, John W. Kelton, Daniel Ray, Mike Edgar, Kye Chisman, and Blaine Emms. Testing of Thermocline Filler Materials and Molten-Salt Heat Transfer Fluids for Thermal Energy Storage Systems in Parabolic Trough Power Plants. *Journal of Solar Energy Engineering*, 127(1):109–116, February 2005.

[17] G. Angelini, A. Lucchini, and G. Manzolini. Comparison of Thermocline Molten Salt Storage Performances to Commercial Two-tank Configuration. *Energy Procedia*, 49:694–704, January 2014.

[18] Jaume Fitó, Sacha Hodencq, Julien Ramousse, Frédéric Wurtz, Benoit Stutz, François Debray, and Benjamin Vincent. Energy- and exergy-based optimal designs of a low-temperature industrial waste heat recovery system in district heating. *Energy Conversion and Management*, 211:112753, May 2020.

[19] Iñigo Ortega-Fernández and Javier Rodríguez-Aseguinolaza. Thermal energy storage for waste heat recovery in the steelworks: The case study of the REslag project. *Applied Energy*, 237:708–719, March 2019.

[20] Aubin Touzo, Régis Olives, Guilhem Dejean, Doan Pham Minh, Mouna El Hafi, Jean-François Hoffmann, and Xavier Py. Experimental and numerical analysis of a packed-bed thermal energy storage system designed to recover high temperature waste heat: an industrial scale up. *Journal of Energy Storage*, 32:101894, December 2020.

[21] Zhen Yang and Suresh V. Garimella. Thermal analysis of solar thermal energy storage in a molten-salt thermocline. *Solar Energy*, 84(6):974–985, June 2010.

[22] Stefano Soprani, Fabrizio Marongiu, Ludvig Christensen, Ole Alm, Kenni Dinesen Petersen, Thomas Ulrich, and Kurt Engelbrecht. Design and testing of a horizontal rock bed for high temperature thermal energy storage. *Applied Energy*, 251:113345, October 2019.

[23] A. Bruch, J. F. Fourmigué, and R. Couturier. Experimental and numerical investigation of a pilot-scale thermal oil packed bed thermal storage system for CSP power plant. *Solar Energy*, 105:116–125, July 2014.

[24] M. T. Zarrinehkafsh and S. M. Sadrameli. Simulation of fixed bed regenerative heat exchangers for flue gas heat recovery. *Applied Thermal Engineering*, 24(2):373–382, February 2004.

[25] Mohammad M. S. Al-Azawii, Carter Theade, Megan Danczyk, Erick Johnson, and Ryan Anderson. Experimental study on the cyclic behavior of thermal energy storage in an air-alumina packed bed. *Journal of Energy Storage*, 18:239–249, August 2018.

[26] J. F. Hoffmann, T. Fasquelle, V. Goetz, and X. Py. Experimental and numerical investigation of a thermocline thermal energy storage tank. *Applied Thermal Engineering*, 114:896–904, March 2017.

[27] Thibaut Esence, Arnaud Bruch, Jean-François Fourmigué, and Benoit Stutz. A versatile one-dimensional numerical model for packed-bed heat storage systems. *Renewable Energy*, 133:190–204, April 2019.

[28] S. Vannerem, P. Neveu, and Q. Falcoz. Experimental and numerical investigation of the impact of operating conditions on thermocline storage performance. *Renewable Energy*, 168:234–246, May 2021.

[29] M. Moradi, M. Farrokhi, A. Rahimi, and M. S. Hatamipour. Modeling strategies for sensible heat thermal energy recovery through packed beds. *Journal of Energy Storage*, 54:105297, October 2022.

[30] T. Fasquelle, Q. Falcoz, P. Neveu, and J. F. Hoffmann. A temperature threshold evaluation for thermocline energy storage in concentrated solar power plants. *Applied Energy*, 212:1153–1164, February 2018.

[31] N. Lopez Ferber, Q. Falcoz, D. Pham Minh, J. F. Hoffmann, A. Meffre, A. Nzihou, and V. Goetz. Flexibility and robustness of a high-temperature air/ceramic thermocline heat storage pilot. *Journal of Energy Storage*, 21:393–404, February 2019.

[32] Aubin Touzo, Régis Olives, Guilhem Dejean, Doan Pham Minh, and Mouna El Hafi. Influence of solar heat sources on packed bed TES performances. In *Proceedings of Solar PACES 2020*, Albuquerque, USA, October 2020.

[33] Aubin Touzo. *Intégration d'un stockage thermocline à des procédés énergétiques*. PhD thesis, Université de Perpignan Via Domitia, Perpignan, May 2021.

[34] S. E. Faas, L. R. Thorne, E. A. Fuchs, and N. D. Gilbertsen. 10 MW/sub e/ Solar Thermal Central Receiver Pilot Plant: thermal storage subsystem evaluation. Final report. Technical Report SAND86-8212, Sandia National Lab. (SNL-CA), Livermore, CA (United States), United States, June 1986.

[35] James E. Pacheco, Steven K. Showalter, and William J. Kolb. Development of a Molten-Salt Thermocline Thermal Storage System for Parabolic Trough Plants. *Journal of Solar Energy Engineering*, 124(2):153–159, May 2002.

[36] Simone A. Zavattoni, Giw Zanganeh, Andrea Pedretti, and Maurizio C. Barbato. Numerical analysis of the packed bed TES system integrated into the first parabolic trough CSP pilot-plant using air as heat transfer fluid. *AIP Conference Proceedings*, 2033(1):090027, November 2018. Publisher: American Institute of Physics.

[37] Christian Odenthal, Wolf-Dieter Steinmann, and Stefan Zunft. Analysis of a horizontal flow closed loop thermal energy storage system in pilot scale for high temperature applications – Part I: Experimental investigation of the plant. *Applied Energy*, 263:114573, April 2020.

[38] Christian Odenthal, Wolf-Dieter Steinmann, and Stefan Zunft. Analysis of a horizontal flow closed loop thermal energy storage system in pilot scale for high temperature applications – Part II: Numerical investigation. *Applied Energy*, 263:114576, April 2020.

[39] Thibaut Esence, Arnaud Bruch, Sophie Molina, Benoit Stutz, and Jean-François Fourmigué. A review on experience feedback and numerical modeling of packed-bed thermal energy storage systems. *Solar Energy*, 153:628–654, September 2017.

[40] K. A. R. Ismail and R. Stuginsky Jr. A parametric study on possible fixed bed models for pcm and sensible heat storage. *Applied Thermal Engineering*, 19(7):757–788, July 1999.

[41] J. F. Hoffmann, T. Fasquelle, V. Goetz, and X. Py. A thermocline thermal energy storage system with filler materials for concentrated solar power plants: Experimental data and numerical model sensitivity to different experimental tank scales. *Applied Thermal Engineering*, 100:753–761, May 2016.